A Constrained Optimization Approach to Compander Design for OFDM PAPR Reduction

Stephen P. DelMarco, *Member, IEEE*

***Abstract*—In this paper, we derive new multi-component companders for reducing peak-to-average power ratio (PAPR) in orthogonal frequency-division multiplexing signals, using a constrained optimization approach. The new companders provide out-of-band power rejection performance improvements over current state-of-the art companders, while maintaining comparable demodulation performance. The newly designed companders are derived by minimally perturbing the Rayleigh signal amplitude distribution, while enforcing the constant power and probability density function constraints. The use of a multi-component approach to compander construction provides design flexibility, and expands the space of tradeoffs between demodulation performance, PAPR reduction, and out-of-band power rejection. Furthermore, the new companders provide solutions in operating regions where certain current companders fail to exist due to violation of one or more constraints; for example, solutions may be derived for cutoff amplitude values that are unobtainable using other companders. We formulate the constrained optimization problem for compander design and derive the compander and decompander forms. Through numerical simulation, we generate performance results demonstrating the capability of the new companders.**

***Index Terms*—Nonlinear companding transform, orthogonal frequency division multiplexing (OFDM), peak-to-average power ratio (PAPR).**

I. Introduction

IT IS well known that Orthogonal Frequency-Division Multiplexing (OFDM) suffers from a large peak-to-average power ratio (PAPR) problem. For a sufficiently large number of sub-carriers, OFDM signal values are Gaussian-distributed, by the central limit theorem. The Gaussian distributed signal components generate Rayleigh distributed signal amplitude values. The long tail of the Rayleigh distribution indicates the presence of large amplitude values, resulting from constructive interference. These large amplitude values can saturate the power amplifier, used to increase transmission power, thus creating signal distortion which reduces demodulation performance.

Many techniques have been developed to mitigate the PAPR problem. Excellent surveys and overviews are provided in [23] and [24]. Of these techniques, signal companding approaches are attractive because of their simplicity and effectiveness. Companders apply an amplitude weight to the signal, generally downweighting large amplitude values, while upweighting smaller values to maintain constant average power. The large amplitude downweighting, while simultaneously maintaining the same power level, reduces the PAPR. The amplitude weighting introduces signal distortion, so it is important to design companders that introduce minimal distortion to limit demodulation errors, while also providing out-of-band power rejection.

Early solutions adapted companders from speech and audio coding, such as the μ-law and A-law companders [1]–[4]. Recently, these have been extended to provide improved companding performance by adapting compander parameter values or compander form across different amplitude ranges [30], [42]. These early companders were followed by approaches which modified the OFDM signal directly to explicitly define companders using, for example, piecewise linear components [6]–[11], [25], hyperbolic functions [5], [15], or Airy functions [26].

More modern approaches transform the Rayleigh amplitude distribution, or portions of it, into more favorable distributions for companding, such as uniform [12]–[14], [18], trapezoid-like [16], [17], linear [19], [21], inverse square-root [20], or exponential [27]. For higher order QAM modulation, further improvements in compander performance have been obtained by modeling the random power fluctuations due to the symbol amplitude power variation [29].

Another current trend combines companders with other techniques to produce hybrid approaches that improve PAPR reduction performance. Such techniques include precoding, using the Hadamard transform [31]–[33], Discrete Fourier Transform [34], Hartley transform [35], [36], or subcarrier shaping [37], active constellation extension [38], selective mapping [39], and partial transmit sequences [40]. Other approaches augment companding with methods designed to reduce out-of-band interference. Frequency domain filtering, used in an iterative companding approach [41] that performs sequential symbol processing, reduces spectral re-growth. Iterative techniques can provide improved performance over non-iterative techniques, but at the cost of significant additional computation.

Amplitude distribution modification approaches often leave a portion of the Rayleigh distribution unmodified, while applying a reshaping of the Rayleigh distribution tail, for example, using a single linear component [19]. Single-linear component approaches, can suffer from design limitations

Manuscript received May 25, 2017; revised October 13, 2017; accepted October 22, 2017.

The author is with Technology Solutions, BAE Systems, Burlington, MA 01803 USA (e-mail: stephen.delmarco@baesystems.com).

Color versions of one or more of the figures in this paper are available online at http://ieeexplore.ieee.org.

Digital Object Identifier 10.1109/TBC.2017.2781144

due to failure to meet the unity cumulative distribution function (c.d.f) condition. For certain inflection and cutoff point pairs, the probability under the modified probability density function (p.d.f) integrates to a value larger than unity [20].

The success of recent companders, which modify the Rayleigh amplitude distribution, while leaving a portion of the Rayleigh distribution intact, suggests development of compander solutions which minimally perturb the Rayleigh distribution. The inherent flexibility of multi-component companders further suggests designing companders using multiple, piecewise components. In this paper we design companders by transforming the Rayleigh distribution into piecewise linear components in a way that minimally perturbs the Rayleigh amplitude distribution. The flexibility of using multiple components enables design of companders across pairs of inflection and cutoff points where other companders fail to exist, thereby widening the space of possible compander design. We define a constrained optimization problem for amplitude distributions of companded signals to find distributions minimally different from the original Rayleigh amplitude distribution. We solve the optimization problem and derive the associated companders and decompanders. We present numerical simulation results demonstrating compander performance.

The contribution of this paper is three-fold. First, we present a general and straightforward method, based on constrained optimization, for developing families of optimal companders. While we implement the approach for piecewise linear segments, the approach applies to more general amplitude modeling component functions such as polynomials. Second, the realization of the proposed compander generation approach, using piecewise linear segments, generalizes previous single- and double-linear segment companders, thereby providing further flexibility in compander design. Third, the compander realizations developed in this paper provide out-of-band power rejection performance improvements over current companders, thus demonstrating the utility of the proposed approach.

The rest of this paper is organized as follows. Section II defines and solves the constrained optimization problem. Section III presents simulation results and Section IV presents concluding remarks. The appendices contain mathematical details.

II. Compander Design Using Constrained Optimization

This section describes the constrained optimization problem and solution, and presents the compander and decompander.

A. Constrained Optimization Problem Definition

Denote the Rayleigh amplitude distribution by $f_R(x)$ for

$$f_R(x) = \frac{2x}{\sigma^2} e^{-\frac{x^2}{\sigma^2}}.$$

For cutoff value $x = A$, look for a function $g(x)$ which minimizes

$$\int_0^A (f_R(x) - g(x))^2 dx. \tag{1}$$

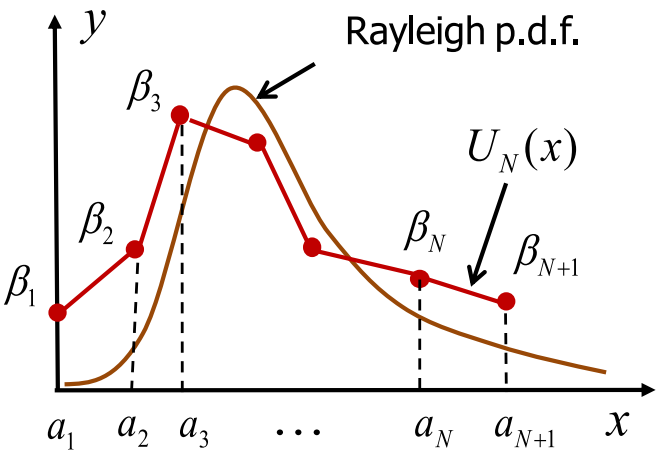

Fig. 1. Piecewise Linear Approximation of Rayleigh Probability Density Function.

Choose $g(x)$ to be of piecewise linear form:

$$g(x) = \sum_{i=1}^{N} U_i(x)$$

where each $U_i(x)$ is a compactly-supported linear segment

$$U_i(x) = \begin{cases} \left(\frac{\beta_{i+1}-\beta_i}{a_{i+1}-a_i}\right)(x - a_i) + \beta_i & \text{for } x \in [a_i, a_{i+1}] \\ 0 & \text{otherwise} \end{cases}, \tag{2}$$

$(a_1, \ldots, a_{N+1})$ is a partition of the interval $[0, A]$ and the β_i are the ordinates at $x = a_i$ (Figure 1).

With the assumed form of $g(x)$, minimize

$$F(\beta_1, \ldots, \beta_{N+1}) = \int_0^A (f_R(x) - g(x))^2 dx \tag{3}$$

as a function of the β_i. There are three constraints on $g(x)$; $g(x)$ is a p.d.f and so must integrate to unity value over $x \in [0, A]$ (i.e., the unity c.d.f. constraint),

$$\int_0^A g(x)dx = 1. \tag{4}$$

The second constraint is the constant power constraint:

$$\int_0^A x^2 g(x)dx = \int_0^\infty x^2 f_R(x)dx = \sigma^2. \tag{5}$$

The third constraint on $g(x)$ is a non-negativity constraint; because $g(x)$ is a p.d.f. it must be non-negative,

$$g(x) \geq 0. \tag{6}$$

In many cases, the non-negativity constraint is automatically satisfied, or nearly satisfied. Therefore, to simplify the solution, we forgo the non-negativity constraint and provide methods to compensate for non-negativity, should it occur. The constrained optimization problem becomes: minimize (3) for the β_i subject to (4) and (5). We solve this problem using Lagrange multipliers.

1) Calculation of Partial Derivatives: Solving the constrained optimization problem, requires calculation of the partial derivatives of F. For

$$F(\beta_1, \ldots, \beta_{N+1}) = \int_0^A \left(f_R(x) - \sum_{i=1}^{N} U_i(x) \right)^2 dx, \tag{7}$$

the integrand in (7) is piecewise continuously differentiable and integrable, thus allowing differentiation under the integral sign. Exploiting the compact support of the $U_i(x)$ produces:

$$\begin{aligned}
\frac{\partial F}{\partial \beta_j} &= \int_0^A \frac{\partial}{\partial \beta_j} \left(f_R(x) - \sum_{i=1}^{N} U_i(x) \right)^2 dx \\
&= \int_0^A 2 \left(f_R(x) - \sum_{i=1}^{N} U_i(x) \right) \left(- \sum_{i=1}^{N} \frac{\partial U_i(x)}{\partial \beta_j} \right) dx \\
&= -2 \int_0^A f_R(x) \sum_{i=1}^{N} \frac{\partial U_i(x)}{\partial \beta_j} dx + 2 \int_0^A \sum_{k=1}^{N} U_k(x) \\
&\quad \times \sum_{i=1}^{N} \frac{\partial U_i(x)}{\partial \beta_j} dx \\
&= -2 \sum_{i=1}^{N} \int_{a_i}^{a_{i+1}} f_R(x) \frac{\partial U_i(x)}{\partial \beta_j} dx + 2 \sum_{i=1}^{N} \int_{a_i}^{a_{i+1}} U_i(x) \\
&\quad \times \frac{\partial U_i(x)}{\partial \beta_j} dx.
\end{aligned} \tag{8}$$

Further simplification of (8) shown in Appendix A produces

$$\frac{\partial F}{\partial \beta_j} = \begin{cases} P_1 \beta_1 + P_2 \beta_2 + P_0 & for\, j = 1 \\ Q_0(j) + Q_1(j) \beta_{j-1} + Q_2(j) \beta_j + Q_3(j) \beta_{j+1} & for\, 1 < j \leq N \\ R_1 \beta_N + R_2 \beta_{N+1} + R_0 & for\, j = N+1 \end{cases} \tag{9}$$

for values $P_0, P_1, P_2, Q_0, Q_1, Q_2, Q_3, R_0, R_1, R_2$ given in Appendix A.

2) Unity C.D.F. Constraint: In Appendix B it is shown that

$$\begin{aligned}
\int_0^A g(x) dx &= \int_0^A \sum_{i=1}^{N} U_i(x) dx \\
&= \sum_{i=1}^{N} T_i^1 \beta_i + T_i^2 \beta_{i+1}
\end{aligned}$$

for values of T_i^1, T_i^2 given in Appendix B. Define

$$g_1(\beta_1, \ldots, \beta_{N+1}) = \sum_{i=1}^{N} T_i^1 \beta_i + T_i^2 \beta_{i+1}. \tag{10}$$

Then, the unity c.d.f. constraint, (4), is expressed as

$$g_1(\beta_1, \ldots, \beta_{N+1}) = 1.$$

3) Constant Power Constraint: In Appendix C it is shown that

$$\begin{aligned}
\int_0^A x^2 g(x) dx &= \int_0^A x^2 \sum_{i=1}^{N} U_i(x) dx \\
&= \sum_{i=1}^{N} W_i^1 \beta_i + W_i^2 \beta_{i+1}
\end{aligned}$$

for values of W_i^1, W_i^2 given in Appendix C. Define

$$g_2(\beta_1, \ldots, \beta_{N+1}) = \sum_{i=1}^{N} W_i^1 \beta_i + W_i^2 \beta_{i+1} \tag{11}$$

then, the constant power constraint (5) becomes

$$g_2(\beta_1, \ldots, \beta_{N+1}) = \sigma^2.$$

4) Lagrangian Definition: Define the Lagrangian as

$$\begin{aligned}
\Lambda(\beta_1, \ldots, \beta_{N+1}, \lambda_1, \lambda_2) &= F(\beta_1, \ldots, \beta_{N+1}) \\
&\quad + \lambda_1 \big[g_1(\beta_1, \ldots, \beta_{N+1}) - 1 \big] \\
&\quad + \lambda_2 \Big[g_2(\beta_1, \ldots, \beta_{N+1}) - \sigma^2 \Big].
\end{aligned}$$

To find the critical point, simultaneously solve the set of equations

$$\begin{aligned}
\frac{\partial \Lambda}{\partial \beta_j} &= \frac{\partial F}{\partial \beta_j} + \lambda_1 \frac{\partial g_1}{\partial \beta_j} + \lambda_2 \frac{\partial g_2}{\partial \beta_j} = 0 \\
\frac{\partial \Lambda}{\partial \lambda_1} &= g_1(\beta_1, \ldots, \beta_{N+1}) - 1 = 0 \\
\frac{\partial \Lambda}{\partial \lambda_2} &= g_2(\beta_1, \ldots, \beta_{N+1}) - \sigma^2 = 0.
\end{aligned}$$

From (10) and (11), we have

$$\begin{aligned}
\frac{\partial g_1}{\partial \beta_j} &= \begin{cases} T_1^1 & for\, j = 1 \\ T_{j-1}^2 + T_j^1 & for\, 1 < j \leq N \\ T_N^2 & for\, j = N+1 \end{cases} \\
\frac{\partial g_2}{\partial \beta_j} &= \begin{cases} W_1^1 & for\, j = 1 \\ W_{j-1}^2 + W_j^1 & for\, 1 < j \leq N \\ W_N^2 & for\, j = N+1 \end{cases}.
\end{aligned} \tag{12}$$

Combining all the partial derivative expressions gives

$$\frac{\partial \Lambda}{\partial \beta_j} = \begin{cases} (P_0 + P_1 \beta_1 + P_2 \beta_2) + \lambda_1 T_1^1 + \lambda_2 W_1^1 & for\, j = 1 \\ \big[Q_0(j) + Q_1(j) \beta_{j-1} + Q_2(j) \beta_j + Q_3(j) \beta_{j+1} \big] & \\ + \lambda_1 \Big(T_{j-1}^2 + T_j^1 \Big) + \lambda_2 \Big(W_{j-1}^2 + W_j^1 \Big) & for\, 1 < j \leq N \\ (R_0 + R_1 \beta_N + R_2 \beta_{N+1}) + \lambda_1 T_N^2 + \lambda_2 W_N^2 & for\, j = N+1 \end{cases}$$

which produces the system of equations in (13) which can be solved numerically, or analytically for small N.

B. Hessian Matrix

Determination of the critical point type, obtained by solving the system (13), as shown at the bottom of the next page, can be obtained from the sign test on the sequence of principal minors of the bordered Hessian [22]. The bordered Hessian of the Lagrangian system is calculated as

$$H = \begin{pmatrix} 0 & 0 & \frac{\partial g_1}{\partial \beta_1} & \cdots & \frac{\partial g_1}{\partial \beta_j} & \cdots & \frac{\partial g_1}{\partial \beta_{N+1}} \\ 0 & 0 & \frac{\partial g_2}{\partial \beta_1} & \cdots & \frac{\partial g_2}{\partial \beta_j} & \cdots & \frac{\partial g_2}{\partial \beta_{N+1}} \\ & \ddots & & & & & \\ & & \ddots & & \frac{\partial^2 F}{\partial \beta_j \partial \beta_i} + \lambda_1 \frac{\partial^2 g_1}{\partial \beta_j \partial \beta_i} + \lambda_2 \frac{\partial^2 g_2}{\partial \beta_j \partial \beta_i} & & \\ & & & \ddots & & & \\ & & & & & & \end{pmatrix}.$$

From (12) and (9) we see that

$$\begin{aligned}
&\frac{\partial^2 g_1}{\partial\beta_j\partial\beta_i} = \frac{\partial^2 g_2}{\partial\beta_j\partial\beta_i} = 0,\\
&\frac{\partial^2 F}{\partial\beta_1^2} = P_1,\ \frac{\partial^2 F}{\partial\beta_2\partial\beta_1} = P_2,\ \frac{\partial^2 F}{\partial\beta_j\partial\beta_1} = 0 \text{ for } j > 2,\\
&\frac{\partial^2 F}{\partial\beta_j^2} = Q_2(j),\ \frac{\partial^2 F}{\partial\beta_{j-1}\partial\beta_j} = Q_1(j),\ \frac{\partial^2 F}{\partial\beta_{j+1}\partial\beta_j} = Q_3(j),\\
&\frac{\partial^2 F}{\partial\beta_k\partial\beta_j} = 0 \text{ for } k \neq \{j-1, j, j+1\},\\
&\frac{\partial^2 F}{\partial\beta_{N+1}^2} = R_2,\ \frac{\partial^2 F}{\partial\beta_N\partial\beta_{N+1}} = R_1,\ \frac{\partial^2 F}{\partial\beta_j\partial\beta_{N+1}} = 0 \text{ for } j < N.
\end{aligned}$$

Performing the sign test numerically shows that the solution to (13) is a minimum.

C. Compander and Decompander

Denote the companding function by C which operates on the input sequence $x(n)$ by modifying the amplitude to produce the companded output sequence $y(n) = C\{x(n)\}$. The compander is monotonic over its domain $x \in [0, A]$, so the compander may be derived as

$$C\{x(n)\} = sgn\{x(n)\}\ F_{|y|}^{-1} F_{|x|}\{x(n)\} \tag{14}$$

where $F_{|x|}$ denotes the c.d.f of the input and $F_{|y|}$ denotes the c.d.f of the output companded signal. To derive the compander, expressions for each c.d.f in (14) are needed. For $a_i \leq x < a_{i+1}$, $i \geq 1$, the compander, derived in Appendix D, is given as

$$F_{|y|}^{-1} F_R(x) = \pm\sqrt{\frac{1 - e^{-\frac{x^2}{\sigma^2}} - Z_{i-1}}{\gamma_i} - \left(\frac{\varepsilon_i}{\gamma_i} - \frac{\delta_i^2}{4\gamma_i^2}\right)} - \frac{\delta_i}{2\gamma_i} \tag{15}$$

where F_R denotes the Rayleigh c.d.f., and for values of $\gamma_i, \delta_i, \varepsilon_i, Z_{i-1}$ given in Appendix D. The decompander results from a straightforward inversion of (15) and is given as:

$$x = \text{sgn}(y)\sqrt{-\sigma^2 \ln\left(-\gamma_i\left(y + \frac{\delta_i}{2\gamma_i}\right)^2 - \varepsilon_i + \frac{\delta_i^2}{4\gamma_i} + 1 - Z_{i-1}\right)}.$$

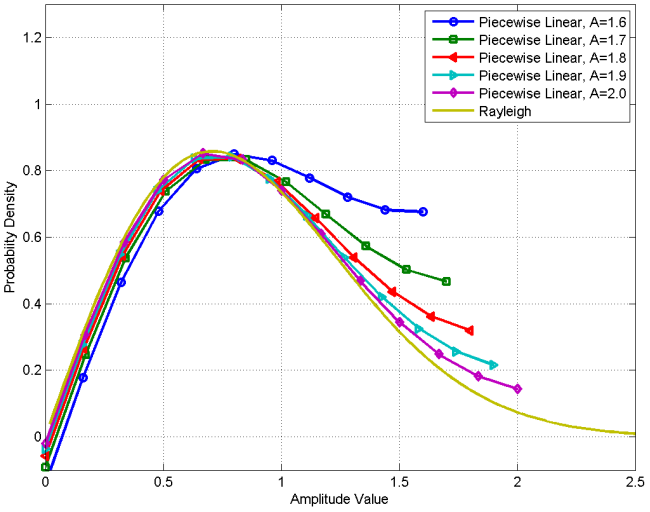

Fig. 2. Optimal Solution versus Rayleigh Distribution for Different Cutoff Values.

III. Numerical Results

A. Numerical Solutions and Analysis

We solve system (13) numerically. Throughout, we take $\sigma = 1.0$ to generate a normalized complex signal with unit power. Figure 2 displays plots of the optimal solution compared against the baseline Rayleigh distribution, as a function of cutoff value $A \in \{1.6, 1.7, 1.8, 1.9, 2.0\}$.

Two observations are clear from Figure 2. As A increases, the solution approaches the baseline Rayleigh distribution. The portion of the optimal solution below the mode of the Rayleigh function shifts leftward toward the Rayleigh distribution front end, while the tail of the optimal solution falls to meet the Rayleigh tail. Larger values of A show that the optimal solution is close to a piecewise linear model of the Rayleigh distribution tail.

The second observation is that the first ordinate, β_1 is negative and thus a portion of the solution has negative values. This condition violates the non-negativity constraint on probability density functions. There are two methods for overcoming the partial negativity of the optimal solution. The first method increases the first abscissa $a_1 = 0$ value to be made small but positive, until β_1 in the solution becomes positive. In this case, the solution consists of the piecewise solution for $x \geq a_1$, and

$$\begin{pmatrix}
T_1^1 & W_1^1 & P_1 & P_2 & 0 & & & & & 0\\
T_1^2 + T_2^1 & W_1^2 + W_2^1 & Q_1(2) & Q_2(2) & Q_3(2) & 0 & & & & 0\\
\vdots & & & & & & & & & \\
T_{j-1}^2 + T_j^1 & W_{j-1}^2 + W_j^1 & 0 & & 0 & Q_1(j) & Q_2(j) & Q_3(j) & 0 & 0\\
\vdots & & & & & & & & & \\
T_N^2 & W_N^2 & 0 & & & & 0 & R_1 & R_2 & \\
0 & 0 & T_1^1 & T_1^2 + T_2^1 & T_2^2 + T_3^1 & \dots & & T_{N-1}^2 + T_N^1 & T_N^2 & \\
0 & 0 & W_1^1 & W_1^2 + W_2^1 & W_2^2 + W_3^1 & \dots & & W_{N-1}^2 + W_N^1 & W_N^2 &
\end{pmatrix}
\begin{pmatrix}
\lambda_1\\ \lambda_2\\ \\ \beta_j\\ \\ \beta_{N-1}\\ \beta_N\\ \beta_{N+1}
\end{pmatrix}
=
\begin{pmatrix}
-P_0\\ -Q_0(2)\\ \vdots\\ -Q_0(j)\\ \vdots\\ -R_0\\ 1\\ \sigma^2
\end{pmatrix} \tag{13}$$

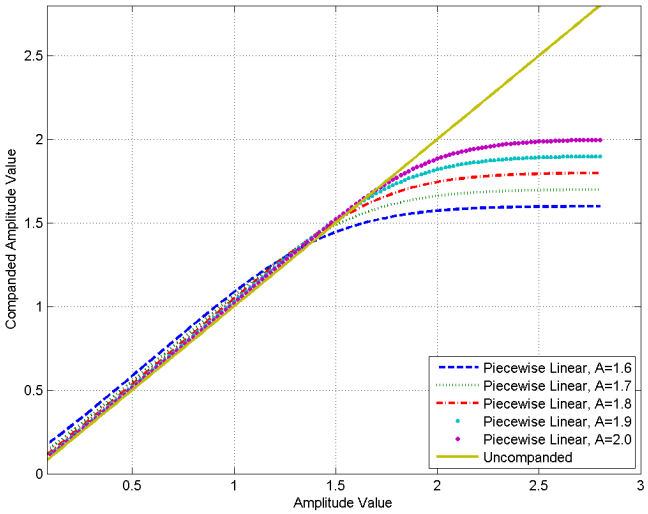

Fig. 3. Companders for Optimal Solutions versus Uncompanded Amplitude.

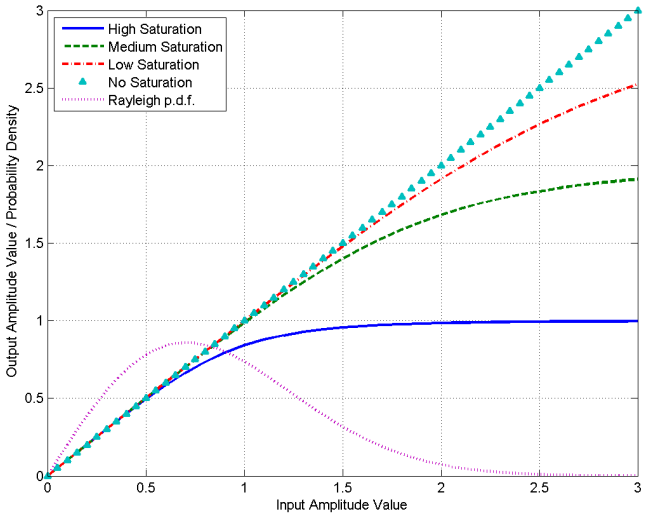

Fig. 4. Power Amplifier Amplitude Curves with Rayleigh Probability Density.

either the undisturbed up-front portion of the Rayleigh distribution for $0 \leq x < a_1$, or simply neglect values smaller than a_1. The perturbation of a_1 is generally small. As an example, the worst case scenario in Figure 2 occurs at $A = 1.6$, for which $\beta_1 \approx 0$ with $\beta_1 > 0$ at $x = .0715$. At this value, $\int_0^x f_R(\xi)\, d\xi \approx .0051$ which is small and may be neglected. The power contribution is even smaller.

The second method uses the Rayleigh distribution as the front segment of the distribution, and perturbs the tail of the optimal solution to meet the new unity c.d.f. and constant power constraints. This perturbation approach is the subject of a future publication.

Companders for each solution are shown in Figure 3.

B. Simulation Results

To evaluate performance of the proposed compander, we generated numerical simulation results for OFDM signals. We used QPSK modulation on 64 and 1024 subcarriers with additive white Gaussian noise (AWGN) and Stanford University Interim-1 (SUI-1) channel models. We use the standard minimum oversampling factor of four to ensure that the PAPR from the discrete signals adequately models the PAPR from continuous signals. A standard deviation of $\sigma = 1.0$ was chosen for the Rayleigh distribution to generate unit power signals. A minimum of ten thousand random signal-plus-noise realizations were generated for each noise level. PAPR is given by

$$PAPR = \frac{\max_n \left(|x_n|^2\right)}{E\left[|x_n|^2\right]}$$

and is quantified by the complimentary cumulative distribution function (CCDF) which gives the probability that the PAPR surpasses a given threshold: $CCDF = prob\,(PAPR > PAPR_0)$. Compander performance was also characterized by bit error rate (BER) versus SNR (E_b/N_0), which measures demodulation performance, and power spectrums, which show out-of-band power rejection.

Experiments with the compander derived in Section II – called the Lagrange compander (LG) - indicated that an

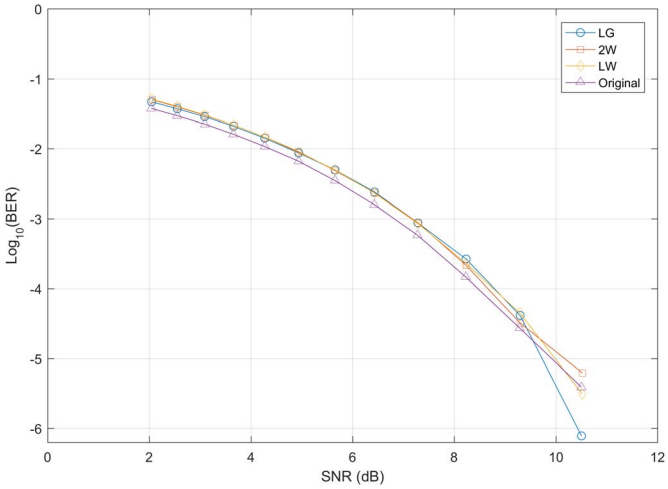

Fig. 5. Bit Error Rate Performance; No Power Amplifier Use, AWGN Channel, 64 Subcarriers.

out-of-band power rejection performance gain occurs for larger cutoff values. LG results were generated and compared against two recent high-performing companders; the linear Wang compander (LW) in [19], and the two-component, piecewise linear Wang compander (2W) in [21]. A cutoff value of $A = 2.1213$ was chosen. For a fair comparison, the optimal 2W compander was chosen and perturbed to reach the chosen cutoff value. The inflection point for the LW compander was calculated to provide a solution for the chosen cutoff value. We generated performance results for two LG companders; a 9-segment, tail-perturbed compander and a 12-segment full-range compander. Piecewise linear component parameter values for the 9-segment LG compander are calculated as:

$$a_i \in \{1.4160, 1.4944, 1.5727, 1.6511, 1.7295, 1.8078, 1.8862, 1.9646, 2.0429, 2.1213\},$$

$$\beta_i \in \{0.3801, 0.2795, 0.2258, 0.1845, 0.1557, 0.1394, 0.1356, 0.1442, 0.1653, 0.1960\}.$$

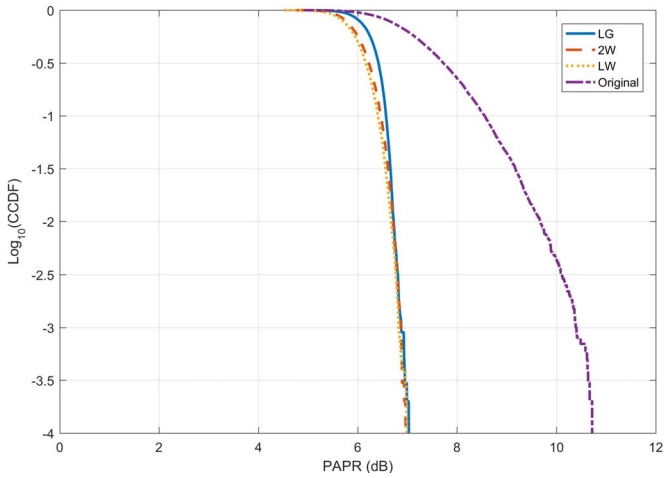

Fig. 6. PAPR Reduction Performance; No Power Amplifier Use, AWGN Channel, 64 Subcarriers.

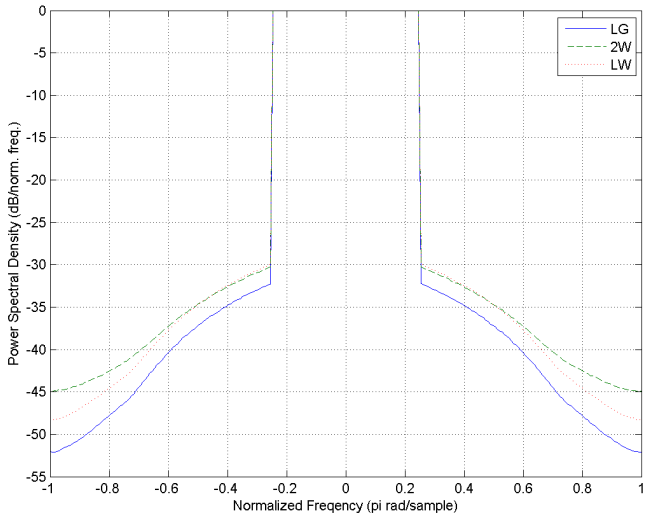

Fig. 7. Out-of-Band Power Rejection; No Power Amplifier Use, AWGN Channel, 64 Subcarriers.

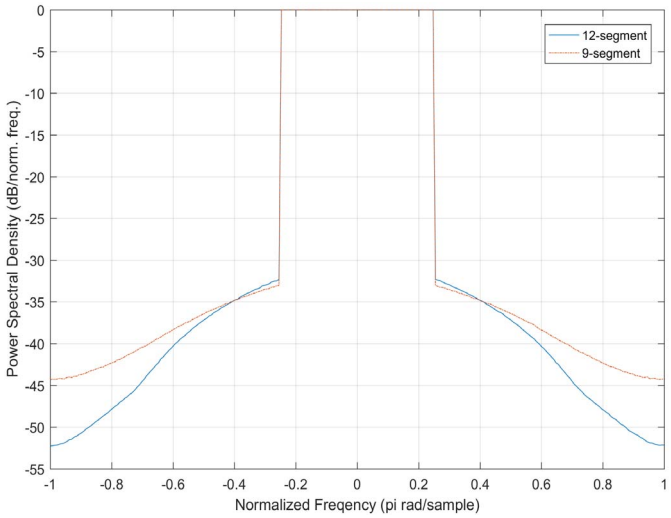

Fig. 8. Out-of-Band Power Rejection; 9-Segment versus 12-Segment LG Companders, No Power Amplifier Use, AWGN Channel, 64 Subcarriers.

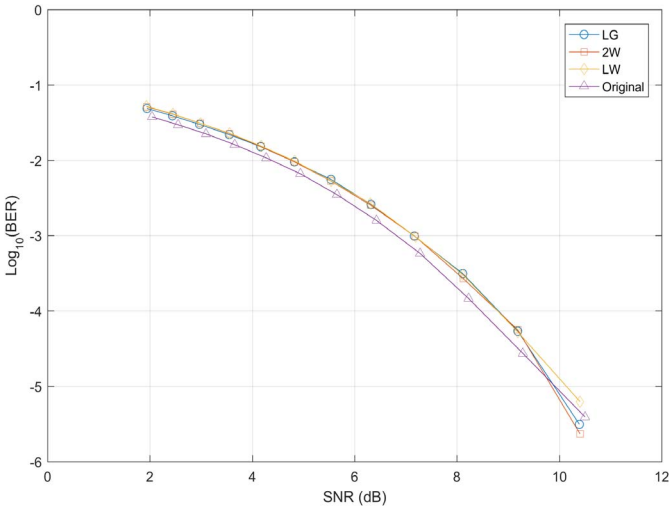

Fig. 9. Bit Error Rate Performance; Low-Level of Power Amplifier Saturation, AWGN Channel, 64 Subcarriers.

Piecewise linear component parameter values for the 12-segment LG compander are calculated as:

$$a_i \in \{0.0055, 0.1818, 0.3581, 0.5345, 0.7108, 0.8871, 1.0634, 1.2397, 1.4160, 1.5924, 1.7687, 1.9450, 2.1213\},$$

$$\beta_i \in \{0.0001, 0.3449, 0.6283, 0.8045, 0.8602, 0.8105, 0.6899, 0.5385, 0.3903, 0.2668, 0.1764, 0.1182, 0.0857\}.$$

The $\gamma_i, \delta_i, \varepsilon_i$ parameters are calculated directly from the a_i, β_i parameters as shown in Appendix D.

Performance results were generated with and without use of a nonlinear, zero-phase power amplifier model [7], [28] in the processing chain. The power amplifier produces the output signal amplitude as a function of the input signal amplitude via

$$|y_{OUT}(t)| = \frac{a|y_{IN}(t)|}{\left[1 + \left(\frac{|y_{IN}(t)|}{A_{SAT}}\right)^{2p}\right]^{\frac{1}{2p}}}$$

where $A_{SAT} \in \{1.0, 2.0, 3.0\}$ denotes the saturation amplitude value, for high-, medium-, and low- saturation levels, respectively, and $p = 2$ characterizes the nonlinearity. Power amplifier amplitude curves are displayed in Figure 4 along with the Rayleigh p.d.f. for gauging the severity of the nonlinearities.

1) AWGN Channel, 64 Subcarriers: Figures 5, 6, and 7 contain, respectively, plots for BER and CCDF, both on logarithmic scales, and out-of-band power rejection for the 12-segment LG, 2W, and LW companders with no power amplifier used, over an AWGN channel with 64 subcarriers. Results show that despite slightly lower PAPR performance of the LG compander, bit error rate performance for all three companders is approximately equal, while the LG compander provides improved out-of-band power rejection. Figure 7 shows that the LG compander provides an out-of-band power rejection performance improvement of more than 1.9 dB, while for distant frequency bins the performance improvement is over 3.8 dB.

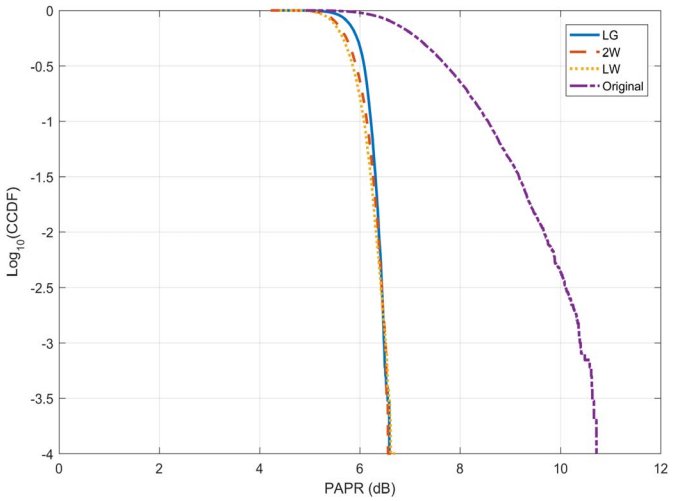

Fig. 10. PAPR Reduction Performance; Low-Level of Power Amplifier Saturation, AWGN Channel, 64 Subcarriers.

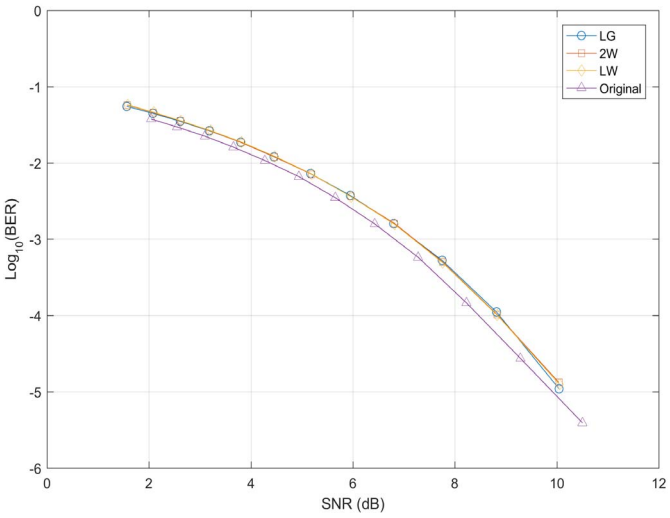

Fig. 12. Bit Error Rate Performance; Medium-Level of Power Amplifier Saturation, AWGN Channel, 64 Subcarriers.

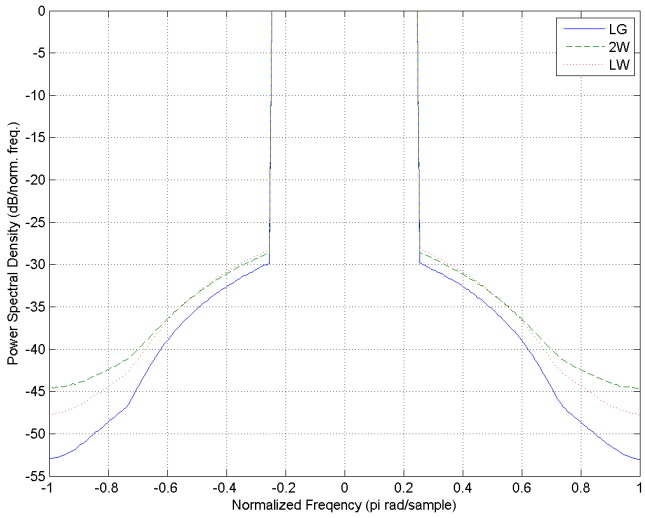

Fig. 11. Out-of-Band Power Rejection; Low-Level of Power Amplifier Saturation, AWGN Channel, 64 Subcarriers.

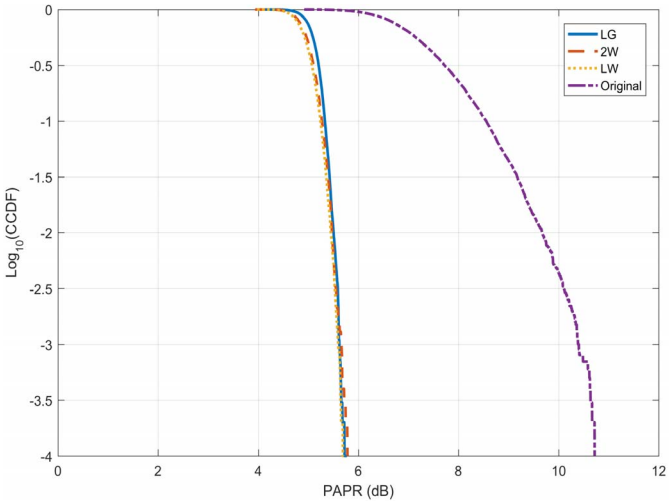

Fig. 13. PAPR Reduction Performance; Medium-Level of Power Amplifier Saturation, AWGN Channel, 64 Subcarriers.

LG compander design provides the flexibility to use different piecewise component breakpoint sets and different numbers of segments. This design flexibility provides different tradeoffs. For example, Figure 8 provides power spectrums for the 9-segment and 12-segment companders. Figure 8 shows that the 12-segment LG compander provides better out-of-band power rejection for distant frequency bins by almost 8 dB. However, the 9-segment LG compander provides a .7 dB improvement at channel edge bins.

Figures 9, 10, and 11 show the effect of low-levels of power amplifier saturation on performance. All three companders provide approximately equal bit error rate performance. The LG compander provides slightly lower PAPR reduction performance, but significantly better out-of-band power rejection; a minimum of over almost 1.3 dB to over 5.2 dB for distant frequency bins.

Figures 12, 13, and 14 contain results for the medium power amplifier saturation level. Again, all three companders provide approximately the same bit error performance. The LG compander provides slightly lower PAPR reduction performance, but significantly improved out-of-band power rejection, particularly for distant frequency bins; a minimum of over .3 dB to over 7. dB. For the large amplifier saturation, the LG compander displays similar performance for PAPR and symbol error rate, but a small degradation in out-of-band power reduction; approximately .07 dB to a maximum of approximately .74 dB.

2) SUI-1 Channel, 64 Subcarriers: Figures 15, 16, and 17 contain BER, CCDF, and power spectrum plots for the three companders over a SUI-1 fading channel, for the low amplifier saturation level $A_{SAT} = 3.0$, using 64 subcarriers. The 9-segment LG compander is used. As for the AWGN channel, Figure 15 shows that the BER performance is approximately the same for all three companders. Figure 16 shows that the LG compander experiences a small PAPR reduction performance loss compared to the LW and 2W companders. However, the power spectrum in Figure 17 shows that

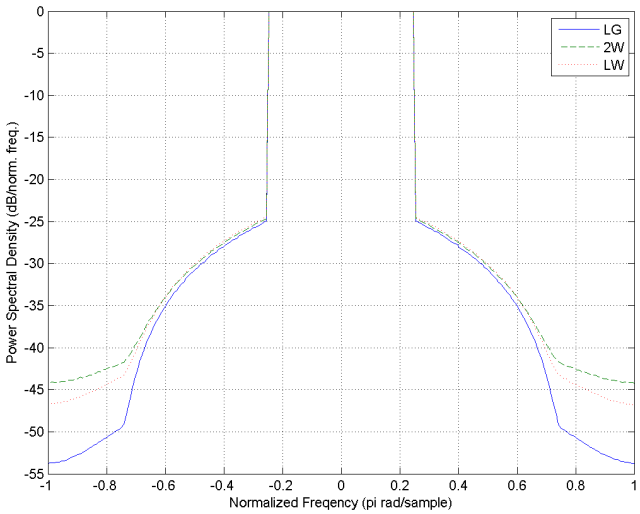

Fig. 14. Out-of-Band Power Rejection; Medium-Level of Power Amplifier Saturation, AWGN Channel, 64 Subcarriers.

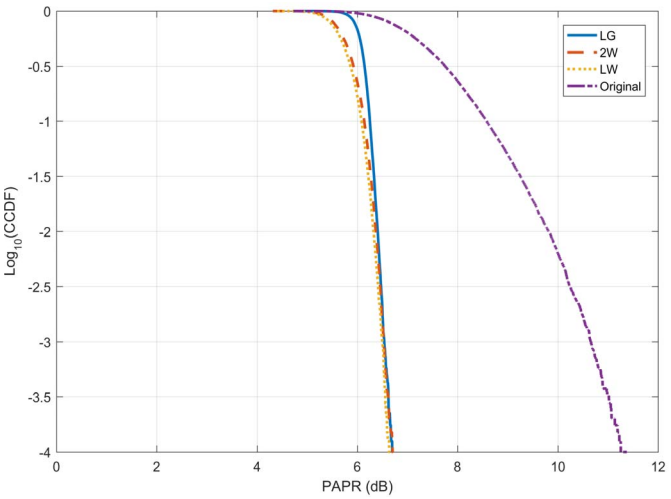

Fig. 16. PAPR Reduction Performance; Low-Level of Power Amplifier Saturation, SUI-1 Channel, 64 Subcarriers.

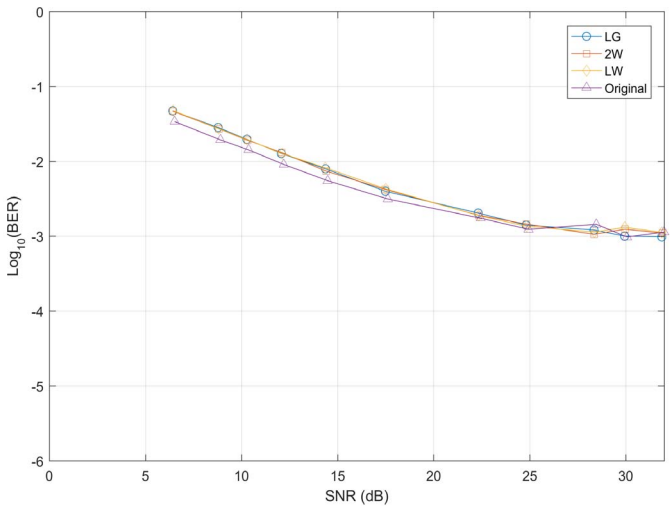

Fig. 15. Bit Error Rate Performance; Low-Level of Power Amplifier Saturation, SUI-1 Channel, 64 Subcarriers.

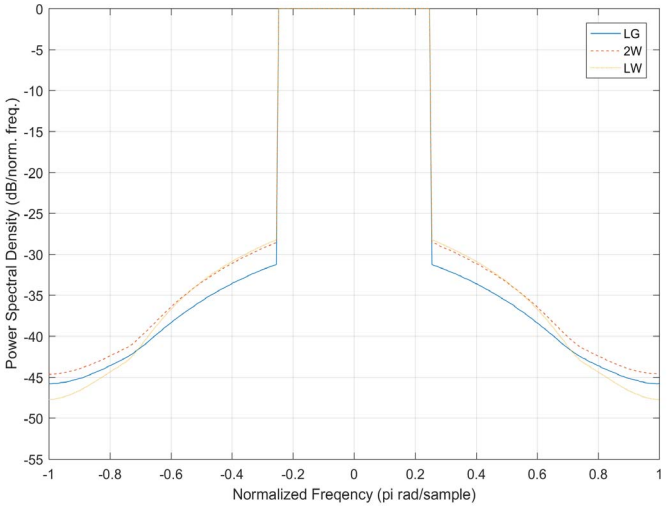

Fig. 17. Out-of-Band Power Rejection; Low-Level of Power Amplifier Saturation, SUI-1 Channel, 64 Subcarriers.

the LG compander provides an out-of-band power rejection performance improvement of over 2.6 dB at the channel edges.

3) SUI-1 Channel, 1024 Subcarriers: Here performance results are presented for the 9-segment LG compander over a SUI-1 fading channel, with low power amplifier saturation, and use of 1024 subcarriers. BER performance for all three companders is approximately equal, but the LG compander provides an out-of-band power rejection performance improvement, at the cost of a small loss in PAPR reduction performance. Figure 18 shows the small PAPR reduction performance loss from the LG compander relative to the other two companders, which is smaller than what occurs over the AWGN channel. However, the power spectrum results in Figure 19 show that the LG compander provides over 2.6 dB in out-of-band power rejection at the channel edges.

C. Computational Complexity

Computational complexity of the LG compander is competitive with modern companders designed using the Rayleigh amplitude distribution modification approach. Most computation can be performed offline, during a pre-transmission stage, to calculate compander and decompander parameter values. The solution of (13) and other parameter value calculation costs on the order of seconds of processing time on a modern laptop. Table I shows the operation counts per signal sample for the LG, LW, 2W, and Kang *et al.* [31] companders. Table II shows the operation counts for the decompanders. The operation counts assume all constant values are pre-calculated for all companders and decompanders, for example, the γ_i, δ_i, ε_i values shown in Appendix D, and the constant expressions using them in (15). The 2W compander has two distinct forms and operation counts for both forms are shown in Tables I and II.

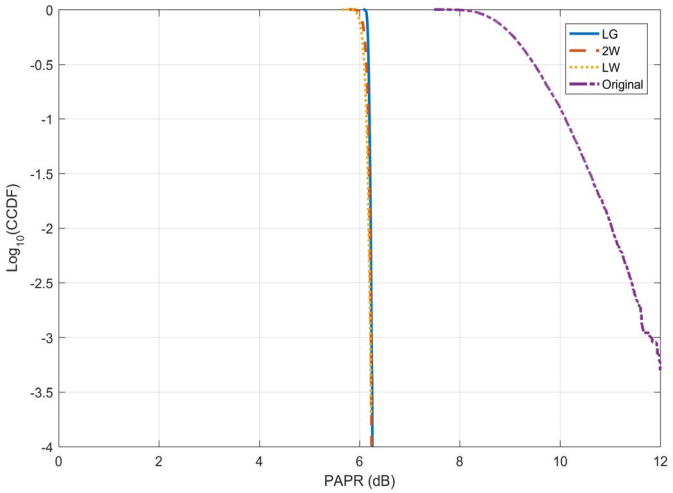

Fig. 18. PAPR Reduction Performance; Low-Level of Power Amplifier Saturation, SUI-1 Channel, 1024 Subcarriers.

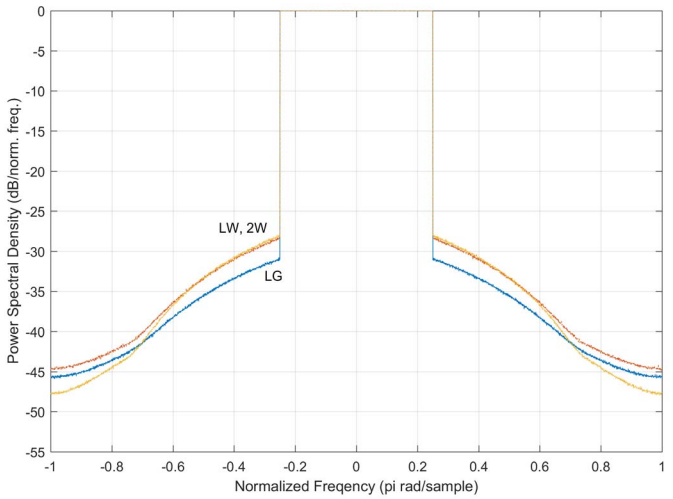

Fig. 19. Out-of-Band Power Rejection; Low-Level of Power Amplifier Saturation, SUI-1 Channel, 1024 Subcarriers.

TABLE I
NUMBER OF COMPANDER FLOATING POINT OPERATIONS PER SIGNAL SAMPLE

Compander Type	$\sqrt{}$	exp	ln	Multiplications	Additions
LG	1	1	0	3	3
LW [19]	1	1	0	4	3
2W [21]	1	1	0	3	1
	1	1	0	4	3
Kang [31], $d=2$	1	1	0	3	1

Companders designed using Rayleigh amplitude distribution modification are generally more computationally costly than companders designed directly in the amplitude value domain, for example [25]. Relative to such companders, companders designed using amplitude distribution modification require one additional square root and one exponentiation operation. The decompanders require an additional square root and logarithm operation. For companders designed using the amplitude distribution modification approach, Tables I and II show that the LG requires approximately the same number of operations as other modern companders.

TABLE II
NUMBER OF DECOMPANDER FLOATING POINT OPERATIONS PER SIGNAL SAMPLE

Decompander Type	$\sqrt{}$	exp	ln	Multiplications	Additions
LG	1	0	1	3	2
LW [19]	1	0	1	4	2
2W [21]	1	0	1	3	1
	1	0	1	4	2
Kang [31], $d=2$	1	0	1	2	3

IV. CONCLUDING REMARKS

In this paper, we developed a family of multi-component companders for PAPR reduction in OFDM signals using a constrained optimization approach. We derived companders and decompanders and demonstrated that the new companders can provide performance improvements over current state-of-the art solutions. The new companders provide an improvement in out-of-band power rejection performance. This performance improvement was shown to persist across channel type, power amplifier use, and number of subcarriers. The new companders can also provide solutions over ranges of the cutoff values where current state-of-the-art companders fail to exist. The set of companders developed in this paper increases the solution space of companders, thereby providing a wider space of tradeoffs between demodulation performance, PAPR reduction, and out-of-band power rejection. Furthermore, the constrained optimization problem formulation and solution developed in this paper for piecewise linear components, is applicable to more general functional forms, thereby further increasing the compander design space.

APPENDIX A

Rewrite $U_i(x)$ as

$$U_i(x) = \left(\frac{x-a_i}{a_{i+1}-a_i}\right)\beta_{i+1} + \left(1-\frac{x-a_i}{a_{i+1}-a_i}\right)\beta_i$$

so that

$$\frac{\partial U_i}{\partial \beta_j} = \left(\frac{x-a_i}{a_{i+1}-a_i}\right)\frac{\partial \beta_{i+1}}{\partial \beta_j} + \left(1-\frac{x-a_i}{a_{i+1}-a_i}\right)\frac{\partial \beta_i}{\partial \beta_j} \quad \text{(A.1)}$$

For $j=1$, and $j=N+1$, (A.1) becomes

$$\frac{\partial U_i}{\partial \beta_1} = \begin{cases} 1-\frac{x-a_1}{a_2-a_1} & \text{if } i=1 \\ 0 & \text{otherwise} \end{cases},$$

$$\frac{\partial U_i}{\partial \beta_{N+1}} = \begin{cases} \frac{x-a_N}{a_{N+1}-a_N} & \text{if } i=N \\ 0 & \text{otherwise} \end{cases}.$$

For $1 < j \le N$, (A.1) becomes

$$\frac{\partial U_i}{\partial \beta_j} = \begin{cases} 1-\frac{x-a_j}{a_{j+1}-a_j} & \text{if } i=j \\ \frac{x-a_{j-1}}{a_j-a_{j-1}} & \text{if } i=j-1 \\ 0 & \text{otherwise} \end{cases}. \quad \text{(A.2)}$$

Using (A.2), substituting the partial derivatives of U_i into (8) gives, for $j = 1$

$$\frac{\partial F}{\partial \beta_1} = -2\int_{a_1}^{a_2} f_R(x)\left(1 - \frac{x-a_1}{a_2-a_1}\right)dx + 2\int_{a_1}^{a_2} U_1(x)\left(1 - \frac{x-a_1}{a_2-a_1}\right)dx$$

for $1 < j \le N$

$$\frac{\partial F}{\partial \beta_j} = -2\int_{a_{j-1}}^{a_j} f_R(x)\left(\frac{x-a_{j-1}}{a_j-a_{j-1}}\right)dx - 2\int_{a_j}^{a_{j+1}} f_R(x)\left(1 - \frac{x-a_j}{a_{j+1}-a_j}\right)dx + 2\int_{a_{j-1}}^{a_j} U_{j-1}(x)\left(\frac{x-a_{j-1}}{a_j-a_{j-1}}\right)dx + 2\int_{a_j}^{a_{j+1}} U_j(x)\left(1 - \frac{x-a_j}{a_{j+1}-a_j}\right)dx$$

and for $j = N+1$

$$\frac{\partial F}{\partial \beta_{N+1}} = -2\int_{a_N}^{a_{N+1}} f_R(x)\left(\frac{x-a_N}{a_{N+1}-a_N}\right)dx + 2\int_{a_N}^{a_{N+1}} U_N(x)\left(\frac{x-a_N}{a_{N+1}-a_N}\right)dx.$$

Straightforward integration and much simplification yields (9) with

$$P_1 = \frac{2\left(a_2 M_1^{U1}(a_1,a_2) - M_1^{U2}(a_1,a_2)\right)}{a_2-a_1}$$

$$P_2 = \frac{2\left(a_2 N_1^{U1}(a_1,a_2) - N_1^{U2}(a_1,a_2)\right)}{a_2-a_1}$$

$$P_0 = \frac{2\left(K_R^2(a_1,a_2) - a_2 K_R^1(a_1,a_2)\right)}{a_2-a_1}.$$

$$Q_0(j) = \left(\frac{2}{a_j-a_{j-1}}\right)\left[-K_R^2(a_{j-1},a_j) + a_{j-1}K_R^1(a_{j-1},a_j)\right] + \left(\frac{2}{a_{j+1}-a_j}\right)\left[K_R^2(a_j,a_{j+1}) - a_{j+1}K_R^1(a_j,a_{j+1})\right]$$

$$Q_1(j) = \left(\frac{2}{a_j-a_{j-1}}\right)\left[M_{j-1}^{U2}(a_{j-1},a_j) - a_{j-1}M_{j-1}^{U1}(a_{j-1},a_j)\right]$$

$$Q_2(j) = \left(\frac{2}{a_j-a_{j-1}}\right)\left[N_{j-1}^{U2}(a_{j-1},a_j) - a_{j-1}N_{j-1}^{U1}(a_{j-1},a_j)\right] + \left(\frac{2}{a_{j+1}-a_j}\right)\left[a_{j+1}M_j^{U1}(a_j,a_{j+1}) - M_j^{U2}(a_j,a_{j+1})\right]$$

$$Q_3(j) = \left(\frac{2}{a_{j+1}-a_j}\right)\left[a_{j+1}N_j^{U1}(a_j,a_{j+1}) - N_j^{U2}(a_j,a_{j+1})\right]$$

$$R_0 = \left(\frac{2}{a_{N+1}-a_N}\right)\left[a_N K_R^1(a_N,a_{N+1}) - K_R^2(a_N,a_{N+1})\right]$$

$$R_1 = \left(\frac{2}{a_{N+1}-a_N}\right)\left[M_N^{U2}(a_N,a_{N+1}) - a_N M_N^{U1}(a_N,a_{N+1})\right]$$

$$R_2 = \left(\frac{2}{a_{N+1}-a_N}\right)\left[N_N^{U2}(a_N,a_{N+1}) - a_N N_N^{U1}(a_N,a_{N+1})\right]$$

$$K_R^1(a_j,a_{j+1}) = e^{-\frac{a_j^2}{\sigma^2}} - e^{-\frac{a_{j+1}^2}{\sigma^2}}$$

$$K_R^2(a_j,a_{j+1}) = a_j e^{-\frac{a_j^2}{\sigma^2}} - a_{j+1}e^{-\frac{a_{j+1}^2}{\sigma^2}} + \frac{\sigma\sqrt{\pi}}{2}\left[\Phi\left(\frac{a_{j+1}}{\sigma}\right) - \Phi\left(\frac{a_j}{\sigma}\right)\right]$$

$$\Phi(x) = \int_0^x \frac{2}{\sqrt{\pi}} e^{-\xi^2} d\xi$$

$$M_j^{U2}(a_j,a_{j+1}) = \frac{1}{6}\left(a_{j+1}^2 + a_j a_{j+1} - 2a_j^2\right)$$

$$N_j^{U2}(a_j,a_{j+1}) = \frac{1}{2}\left(a_{j+1}^2 - a_j^2\right) - M_j^{U2}(a_j,a_{j+1})$$

$$M_j^{U1}(a_j,a_{j+1}) = \frac{1}{2}\left(a_{j+1} - a_j\right)$$

$$N_j^{U1}(a_j,a_{j+1}) = M_j^{U1}(a_j,a_{j+1}).$$

Appendix B

$$\int_0^A g(x)dx = \int_0^A \sum_{i=1}^N U_i(x)dx = \sum_{i=1}^N \int_{a_i}^{a_{i+1}} \left(\frac{\beta_{i+1}-\beta_i}{a_{i+1}-a_i}\right)(x-a_i) + \beta_i dx$$

$$= \sum_{i=1}^N \int_{a_i}^{a_{i+1}} \left(\frac{\beta_{i+1}-\beta_i}{a_{i+1}-a_i}\right)x + \left[\beta_i - \frac{a_i(\beta_{i+1}-\beta_i)}{a_{i+1}-a_i}\right]dx$$

$$= \sum_{i=1}^N \left(\frac{\beta_{i+1}-\beta_i}{a_{i+1}-a_i}\right)\left(\frac{a_{i+1}^2}{2} - \frac{a_i^2}{2}\right) + \left[\beta_i - \frac{a_i(\beta_{i+1}-\beta_i)}{a_{i+1}-a_i}\right](a_{i+1}-a_i).$$

Further simplification produces (10) where:

$$T_i^1 = \frac{a_{i+1}-a_i}{2}, \quad T_i^2 = T_i^1.$$

Appendix C

$$\int_0^A x^2 g(x)dx = \int_0^A x^2 \sum_{i=1}^N U_i(x)dx = \sum_{i=1}^N \int_{a_i}^{a_{i+1}} x^2 U_i(x)dx$$

$$= \sum_{i=1}^N \int_{a_i}^{a_{i+1}} x^2\left(\frac{\beta_{i+1}-\beta_i}{a_{i+1}-a_i}x + \left[\beta_i - \frac{a_i(\beta_{i+1}-\beta_i)}{a_{i+1}-a_i}\right]\right)dx$$

$$= \sum_{i=1}^N \left(\frac{\beta_{i+1}-\beta_i}{a_{i+1}-a_i}\right)\left(\frac{a_{i+1}^4}{4} - \frac{a_i^4}{4}\right) + \left[\beta_i - \frac{a_i(\beta_{i+1}-\beta_i)}{a_{i+1}-a_i}\right]\left(\frac{a_{i+1}^3}{3} - \frac{a_i^3}{3}\right)$$

which, after much simplification, becomes (11) with

$$W_i^1 = \frac{1}{12}\left(a_{i+1}^3 + a_{i+1}^2 a_i + a_i^2 a_{i+1} - 3a_i^3\right),$$
$$W_i^2 = \frac{a_{i+1}^3 - a_i^3}{3} - W_i^1.$$

APPENDIX D

The p.d.f of the companded signal is given by

$$f_{|y|}(x) = \begin{cases} \frac{2x}{\sigma^2} e^{-\frac{x^2}{\sigma^2}} & \text{for } 0 \le x < a_1 \\ f_{a_i}(x) & \text{for } a_i \le x < a_{i+1},\ 1 \le i \le N \\ 0 & \text{for } a_{N+1} \le x \end{cases}.$$

For $a_i \le x < a_{i+1}$, the c.d.f. is given by

$$\begin{aligned} F_{|y|}(x) &= \int_0^x f_{|y|}(\xi)d\xi \\ &= \left[\int_0^{a_1} f_R(\xi)d\xi + \sum_{j=1}^{i-1}\int_{a_j}^{a_{j+1}} f_{a_j}(\xi)d\xi\right] + \int_{a_i}^{x} f_{a_i}(\xi)d\xi \\ &= Z_{i-1} + \int_{a_i}^{x} f_{a_i}(\xi)d\xi \end{aligned} \tag{D.1}$$

where Z_{i-1}denotes the term in brackets. Thus

$$\begin{aligned} F_{|y|}(x) - Z_{i-1} &= \int_{a_i}^{x} f_{a_i}(\xi)d\xi \\ &= \int_{a_i}^{x} m_i\xi + b_i d\xi \\ \text{where } m_i &= \frac{\beta_{i+1} - \beta_i}{a_{i+1} - a_i},\ b_i = \beta_i - \frac{a_i(\beta_{i+1} - \beta_i)}{a_{i+1} - a_i} \\ &= \left(\frac{m_i}{2}\right)x^2 + (b_i)x + \left[-\left(m_i\frac{a_i^2}{2} + b_i a_i\right)\right] \\ &= \gamma_i x^2 + \delta_i x + \varepsilon_i \end{aligned} \tag{D.2}$$

where

$$\gamma_i = \frac{m_i}{2}, \delta_i = b_i, \quad \varepsilon_i = -\left(m_i\frac{a_i^2}{2} + b_i a_i\right).$$

The parameters $\gamma_i, \delta_i, \varepsilon_i$ are calculated directly from the linear segment parameters $(a_1, \ldots, a_{N+1})$ and $(\beta_1, \ldots, \beta_{N+1})$. The a_i are chosen *a priori*, whereas the β_i are obtained from the solution of (13). The a_i may be chosen based on achieving a desired maximum deviation level in (7), where the calculation in (7) uses the $(\beta_1, \ldots, \beta_{N+1})$ obtained from solving (13) given the chosen a_i. For example, start with a set of a_i values which uniformly partition the amplitude range $[0, A]$, determine the associated $(\beta_1, \ldots, \beta_{N+1})$, then calculate the error value from (7). Continue refining the a_i partition until reaching a desired error level in (7).

Now, γ_i might be negative, so divide both sides of (D.2) by γ_i and complete the square to get

$$\left(x + \frac{\delta_i}{2\gamma_i}\right)^2 = \frac{F_{|y|}(x) - Z_{i-1}}{\gamma_i} - \left(\frac{\varepsilon_i}{\gamma_i} - \frac{\delta_i^2}{4\gamma_i^2}\right) \tag{D.3}$$

and thus

$$x = \pm\sqrt{\frac{F_{|y|}(x) - Z_{i-1}}{\gamma_i} - \left(\frac{\varepsilon_i}{\gamma_i} - \frac{\delta_i^2}{4\gamma_i^2}\right)} - \frac{\delta_i}{2\gamma_i}. \tag{D.4}$$

The decision to take the positive or negative square-root in (D.4) results from (D.3) by examining the sign on $x + \frac{\delta_i}{2\gamma_i}$. If positive, choose the positive square-root and if negative choose the negative square-root. Of course, if $x \ge A$, then consider the sign on $A + \frac{\delta_i}{2\gamma_i}$ to make the choice. Finally, the compander is given by $F_{|y|}^{-1}F_R(x)$ which produces the form in (15) for $a_i \le x < a_{i+1}$. To complete the compander derivation, calculate Z_i. From (D1),

$$Z_0 = \int_0^{a_1} f_R(\xi)d\xi = 1 - e^{-\frac{a_1^2}{\sigma^2}}.$$

For $i > 0$, Z_i contains integral terms of the form

$$\int_{a_i}^{a_{i+1}} f_{a_i}(\xi)d\xi$$

which represents a trapezoidal area and can be shown to be

$$\int_{a_i}^{a_{i+1}} f_{a_i}(\xi)d\xi = \frac{\beta_{i+1}(a_{i+1} - a_i) + \beta_i(a_{i+1} - a_i)}{2}.$$

Hence

$$Z_i = Z_{i-1} + \frac{\beta_{i+1}(a_{i+1} - a_i) + \beta_i(a_{i+1} - a_i)}{2}.$$

ACKNOWLEDGMENT

The author would like to express his gratitude to the anonymous reviewers whose suggestions greatly improved the quality and clarity of the paper.

REFERENCES

[1] X. Huang, J. Lu, J. Zheng, J. Chuang, and J. Gu, "Reduction of peak-to-average power ratio of OFDM signals with companding transform," *Electron. Lett.*, vol. 37, no. 8, pp. 506–507, Apr. 2001.

[2] X. Wang, T. T. Tjhung, and C. S. Ng, "Reduction of peak-to-average power ratio of OFDM system using a companding technique," *IEEE Trans. Broadcast.*, vol. 45, no. 3, pp. 303–307, Sep. 1999.

[3] T. G. Pratt, N. Jones, L. Smee, and M. Torrey, "OFDM link performance with companding for PAPR reduction in the presence of non-linear amplification," *IEEE Trans. Broadcast.*, vol. 52, no. 2, pp. 261–267, Jun. 2006.

[4] X. Wang, T. T. Tjhung, C. S. Ng, and A. A. Kassim, "On the SER analysis of a-law companded OFDM system," in *Proc. IEEE GLOBECOM*, vol. 2. San Francisco, CA, USA, 2000, pp. 756–760.

[5] Y. Wang, L.-H. Wang, J.-H. Ge, and B. Ai, "Nonlinear companding transform technique for reducing PAPR of OFDM signals," *IEEE Trans. Consum. Electron.*, vol. 58, no. 3, pp. 752–757, Aug. 2012.

[6] Y. Rahmatallah, N. Bouaynaya, and S. Mohan, "Bit-error-rate performance of companding transforms for OFDM," *IEEE Trans. Veh. Technol.*, vol. 62, no. 8, pp. 4116–4120, Oct. 2013.

[7] S. A. Aburakhia, E. F. Badran, and D. A. E. Mohamed, "Linear companding transform for the reduction of peak-to-average power ratio of OFDM signals," *IEEE Trans. Broadcast.*, vol. 55, no. 1, pp. 155–160, Mar. 2009.

[8] X. Huang, J. Lu, J. Zheng, K. B. Letaief, and J. Gu, "Companding transform for reduction in peak-to-average power ratio of OFDM signals," *IEEE Trans. Wireless Commun.*, vol. 3, no. 6, pp. 2030–2039, Nov. 2004.

[9] C.-L. Wang and S.-J. Ku, "A low-complexity companding transform for peak-to-average power ratio reduction in OFDM systems," in *Proc. IEEE ICASSP*, vol. 4. Toulouse, France, 2006, pp. 329–332.

[10] P. Yang and A. Hu, "Two-piecewise companding transform for PAPR reduction of OFDM signals," in *Proc. 7th Int. Conf. Wireless Commun. Mobile Comput. (IWCMC)*, Istanbul, Turkey, 2011, pp. 619–623.
[11] V. Tabatabavakili and A. Zahedi, "Reduction in peak to average power ratio of OFDM signals using a new continuous linear companding transform," in *Proc. IEEE Int. Symp. Telecommun.*, Tehran, Iran, 2010, pp. 426–430.
[12] T. Jiang, W. Xiang, P. C. Richardson, D. Qu, and G. Zhu, "On the nonlinear companding transform for reduction in PAPR of MCM signals," *IEEE Trans. Wireless Commun.*, vol. 6, no. 6, pp. 2017–2021, Jun. 2007.
[13] T. Jiang, W. Yao, P. Guo, Y. Song, and D. Qu, "Two novel nonlinear companding schemes with iterative receiver to reduce PAPR in multi-carrier modulation systems," *IEEE Trans. Broadcast.*, vol. 52, no. 2, pp. 268–273, Jun. 2006.
[14] T. Jiang, Y. Yang, and Y.-H. Song, "Exponential companding technique for PAPR reduction in OFDM systems," *IEEE Trans. Broadcast.*, vol. 51, no. 2, pp. 244–248, Jun. 2005.
[15] Y. Wang, J.-H. Ge, L.-H. Wang, and B. Ai, "Nonlinear companding transform using hyperbolic tangent function in OFDM systems," in *Proc. WiCOM*, Shanghai, China, 2012, pp. 1–4.
[16] S.-S. Jeng and J.-M. Chen, "Efficient PAPR reduction in OFDM systems based on a companding technique with trapezium distribution," *IEEE Trans. Broadcast.*, vol. 57, no. 2, pp. 291–298, Jun. 2011.
[17] J. Hou, J. H. Ge, and J. Li, "Trapezoidal companding scheme for peak-to-average power ratio reduction of OFDM signals," *Electron. Lett.*, vol. 45, no. 25, pp. 1349–1351, Dec. 2009.
[18] J. Hou, J. Ge, D. Zhai, and J. Li, "Peak-to-average power ratio reduction of OFDM signals with nonlinear companding scheme," *IEEE Trans. Broadcast.*, vol. 56, no. 2, pp. 258–262, Jun. 2010.
[19] Y. Wang, L.-H. Wang, J.-H. Ge, and B. Ai, "An efficient nonlinear companding transform for reducing PAPR of OFDM signals," *IEEE Trans. Broadcast.*, vol. 58, no. 4, pp. 677–684, Dec. 2012.
[20] S. P. DelMarco, "General closed-form family of companders for PAPR reduction in OFDM signals using amplitude distribution modification," *IEEE Trans. Broadcast.*, vol. 60, no. 1, pp. 102–109, Mar. 2014.
[21] Y. Wang, J.-H. Ge, L.-H. Wang, J. Li, and B. Ai, "Nonlinear companding transform for reduction of peak-to-average power ratio in OFDM systems," *IEEE Trans. Broadcast.*, vol. 59, no. 2, pp. 369–375, Jun. 2013.
[22] D. G. Luenberger and Y. Ye, *Linear and Nonlinear Programming*. New York, NY, USA: Springer, 2008.
[23] G. Wunder, R. F. H. Fischer, H. Boche, S. Litsyn, and J.-S. No, "The PAPR problem in OFDM transmission," *IEEE Signal Process. Mag.*, vol. 30, no. 6, pp. 130–144, Nov. 2013.
[24] Y. Rahmatallah and S. Mohan, "Peak-to-average power ratio reduction in OFDM systems: A survey and taxonomy," *IEEE Commun. Surveys Tuts.*, vol. 15, no. 4, pp. 1567–1592, 4th Quart., 2013.
[25] M. Hu, Y. Li, W. Wang, and H. Zhang, "A Piecewise linear companding transform for PAPR reduction of OFDM signals with companding distortion mitigation," *IEEE Trans. Broadcast.*, vol. 60, no. 3, pp. 532–539, Sep. 2014.
[26] Y. Jiang, "New companding transform for PAPR reduction in OFDM," *IEEE Commun. Lett.*, vol. 14, no. 4, pp. 282–284, Apr. 2010.
[27] M. Hu, Y. Li, Y. Liu, and H. Zhang, "Parameter-adjustable piecewise exponential companding scheme for peak-to-average power ratio reduction in orthogonal frequency division multiplexing systems," *IET Commun.*, vol. 8, no. 4, pp. 530–536, Mar. 2014.
[28] S. C. Thompson, J. G. Proakis, and J. R. Zeidler, "The effectiveness of signal clipping for PAPR and total degradation reduction in OFDM systems," in *Proc. IEEE GLOBECOM*, vol. 5. St. Louis, MO, USA, 2005, pp. 2807–2811.
[29] S. Mazahir and S. A. Sheikh, "On companding schemes for PAPR reduction in OFDM systems employing higher order QAM," *IEEE Trans. Broadcast.*, vol. 62, no. 3, pp. 716–726, Sep. 2016.
[30] N. Ali, R. Almahainy, A. Al-Shabili, N. Almoosa, and R. Abd-Alhameed, "Analysis of improved μ-law companding technique for OFDM systems," *IEEE Trans. Consum. Electron.*, vol. 63, no. 2, pp. 126–134, May 2017.
[31] C. Kang, Y. Liu, M. Hu, and H. Zhang, "A low complexity PAPR reduction method based on FWFT and PEC for OFDM systems," *IEEE Trans. Broadcast.*, vol. 63, no. 2, pp. 416–425, Jun. 2017.
[32] J. Xiao *et al.*, "Hadamard transform combined with companding transform technique for PAPR reduction in an optical direct-detection OFDM system," *IEEE/OSA J. Opt. Commun. Netw.*, vol. 4, no. 10, pp. 709–714, Oct. 2012.
[33] B. Elmaroud, A. Faqihi, M. Abbad, and D. Aboutajdine, "PAPR reduction of FBMC signals by combining exponential companding and hadamard transforms," in *Proc. Int. Symp. Netw. Comput. Commun.*, Hammamet, Tunisia, 2014, pp. 1–4.
[34] A. S. Lakamana and A. M. Prasad, "An effective composite PAPR reduction technique of OFDM by using DFT precoding with piecewise linear companding," in *Proc. Int. Conf. Commun. Electron. Syst.*, Coimbatore, India, 2016, pp. 1–6.
[35] A. Thammana and M. K. Kasi, "Improvement measures of DHT precoded OFDM over WiMAX channels with piecewise linear companding," in *Proc. IEEE Annu. India Conf.*, 2016, pp. 1–6.
[36] R. Ghahremani and M. G. Shayesteh, "BER performance improvement and PAPR reduction in OFDM systems based on combined DHT and μ-law companding," in *Proc. Iran. Conf. Elect. Eng.*, Tehran, Iran, 2014, pp. 1483–1487.
[37] P. Elavarasan, G. Nagarajan, and A. Narayanan, "PAPR reduction in MIMO-OFDM systems using joint channel estimation and precoding," in *Proc. Int. Conf. Adv. Commun. Control Comput. Technol.*, Ramanathapuram, India, 2012, pp. 327–331.
[38] A. Hekkala, S. Boumard, and M. Lasanen, "Exponential companding and active constellation extension comparisons for PAPR reduction," in *Proc. Int. Teletraffic Congr.*, Karlskrona, Sweden, 2014, pp. 1–5.
[39] G. S. Toor, H. Singh, and A. S. Bhandari, "PAPR reduction and BER improvement by using logarithmic companding hybrid with SLM technique in bit interleaved COFDM system," in *Proc. Int. Conf. Confluence Next Gener. Inf. Technol. Summit*, Noida, India, 2014, pp. 604–608.
[40] T. Sravanti and N. Vasantha, "A hybrid technique to reduce PAPR in OFDM systems," in *Proc. Int. Conf. Adv. Elect. Electron. Inf. Commun. Bio Informat.*, Chennai, India, 2017, pp. 416–421.
[41] Y. Wang, C. Yang, and B. Ai, "Iterative companding transform and filtering for reducing PAPR of OFDM signal," *IEEE Trans. Consum. Electron.*, vol. 61, no. 2, pp. 144–150, May 2015.
[42] X. Zhang, P. Liu, J. Liu, and S. Liu, "An advanced A-law companding algorithm in VLC-OFDM," in *Proc. IEEE Glob. Conf. Consum. Electron.*, Tokyo, Japan, 2014, pp. 721–722.

Stephen P. DelMarco (M'91) received the B.A. and M.A. degrees in mathematics from Boston College, Boston, MA, USA, in 1981 and the Ph.D. degree in mathematics from Boston University, Boston, MA, USA, in 1985.

He joined Raytheon Company, Bedford, MA, USA, where he performed missile systems and radar signal processing simulation and performance analysis, in 1986. He joined Aware, Inc., Bedford, MA, USA, where he led various efforts in applying wavelets to signal and image processing problems, and performed research and development in biometrics, in 1992. Since joining BAE Systems, Burlington, MA, USA, in 2003, he has been performing research and development in statistical target tracking, automatic target detection and recognition, multisensor data fusion and image registration, sensor modeling, and communications signal processing.

Dr. DelMarco was a recipient of the BAE Systems Joseph G. Wohl Achievement Award for best published technical paper in 2005. He has over 40 publications in peer-reviewed journals and conferences, lightly reviewed conferences, and closed industry conferences, in applied mathematics, mathematical modeling, and signal and image processing.